Exp. Theo. NANOTECHNOLOGY 4 (2020) 1– 10 https://doi.org/10.56053/4.1.1

Optical properties of TiO_2 Nanofibers

*K. -O. Ong, J. Cheong, -F. Heong**

Department of Materials Science and Engineering, National University of Singapore, Singapore 117576, Singapore
*E-mail: fheong@nus.edu.sg

Received 11/2/2019, *Accepted* 30/10/2019, *Published* 15/1/2020

The anatase TiO_2 nanofibers of average diameters 60, 100, and 150 nm were fabricated by controlled electrospinning of a polymeric solution and subsequent sintering of the as-spun fibers. The sintered fibers were polycrystalline and composed of densely packed TiO_2 grains of size ~12 nm. The rutile phase nucleated at the particle interface of the dense anatase TiO_2 nanofibers at a temperature of <570 ℃ because of the increased surface stress observed in these nanofibers. X-ray and electron diffraction measurements and analysis of the sintered fibers showed that the lattice strain increased with a decrease in the fiber diameter. The diameter-dependent lattice strain is attributed to the increased surface energy in fibers of lower diameter. The strain most likely originates from interplay of the surface charge and grain boundary effects. The absorption spectra of the fibers showed a red shift with an increase in the fiber diameter, which is attributed to an increase in the surface stress with a decrease in the fiber diameter.

Keywords: Optical; Metal oxide; Nanofiber.

1. INTRODUCTION

Nanostructured anatase TiO_2 have received much attention recently [1] owing to their promising physical properties for applications in photocatalysis [2] and as electrodes in dye- sensitized solar cells (DSSC) [3]. The photocatalysis and electrical transport properties are closely related to the electronic band gap of the materials. The electronic band gap is affected by the particle size [4-7], shape [8, 9], impurities, surface charges [10] and phase transitions [11]. A large percentage nanofiber is preferable over sintered nanoparticles because these one-dimensional nanostructures can act as guided electron channels in electrodes made up of them. Several groups developed DSSC based on anatase TiO_2 nanofibers [12, 13]. For TiO_2 fibers of 50–150 nm, surface effects are prominent compared to the quantum confinement effects because of the wider band gap of TiO_2. Several techniques have been developed for the fabrication of one-dimensional TiO_2 nanostructures, viz., template of atoms is at the surface of nanometer-sized particles. The growth [14, 15], self-assembling [16, 17], thermal evaporation [18], strong surface

atoms play a major role in their local and global band structures. For the application of TiO_2 as electrodes in DSSC, alkali treatment, and electrospinning. Among these techniques, electrospinning offers advantages of simplicity [19-21], process controllability, low production cost, and scalability for producing industrial quantities. In the electrospinning process, nanofibers of metal oxides are produced from a polymeric solution injected through an electrical field of several kilovolts per centimeter, followed by controlled evaporation of the polymer, calcination, and sintering [22]. The fiber diameter and morphology could be tailored by control- ling the injection rate and electric field. The fiber diameter also depends on the intrinsic properties of the polymeric solution such as the viscosity and surface charge [21]. Electro- spinning of the sol–gel precursor has been employed to produce nanofibers of several technologically important ceramic systems including TiO_2 [22,23]. However, no attempt has so far been made to study the properties of TiO_2 fibers by varying the fiber diameter. In particular, little is known about the correlations between the nanofiber diameter and the optical band-gap energy. Note that the anatase plays a key role in the injection process of DSSC with high conversion efficiency;[3] therefore, knowledge of the phase transition in nanofibers is essential for fabrication of solar cells of higher efficiency. This requirement is further fueled by the fact that there is a considerable difference between the band-gap energies of the anatase and rutile phases [11]. We have now developed TiO_2 nanofibers in the diameter range of 60–150 nm by controlled electrospinning and subsequent sintering. The sintered fibers were highly dense and polycrystalline and consist of uniform grains of average diameter $\sim 12\,\mathrm{nm}$. All of the three fibers of different diameters were constructed from grains of similar diameter by sintering the as-spun fibers under similar conditions for shorter duration. Sintering at lower temperatures for shorter duration also eliminated the grain coarsening. An anatase to rutile structural transformation was found to occur in the nanofibers at temperatures as low as 570 °C. Because of the higher density of the anatase nanofiber, the nucleation of the anatase phase at such lower temperatures occurs at the interfaces. Lattice strains were observed along the grain boundaries of the polycrystalline fiber, which would most likely be the reason for the early nucleation of the rutile phase. The X-ray diffraction (XRD) measurements and subsequent Rietveld analysis showed that the strains in the lattice decrease with an increase in the fiber diameter. The absorption spectra of these fibers showed a red shift with an increase in the fiber diameter. The excitonic peak in the absorption spectra showed a shift of $\sim 15\,\mathrm{nm}$ when the diameter of the fiber increased from 60 to 150 nm. No complementary shift in emission spectra was observed. The observed shift in the absorption spectra has been attributed to the increased surface stress and the consequent lattice strain.

2. EXPERIMENTAL SECTION

The TiO_2 nanofibers were fabricated by electrospinning a mixture of TiO_2 sol and poly (vinylpyrrolidone) (PVP; M_W) 1 300 000, Sigma-Aldrich) polymer. A typical synthesis route here is as follows. First, the TiO_2 sol was prepared by hydrolyzing 0.25 g of titanium tetraisopropoxide [$Ti(O^iPr)_4$; 97%, Sigma-Aldrich] with a mixture of 1 mL of ethanol (98%) and 1 mL of acetic acid (100%, BDH, AnalaR). Next, PVP (~9 wt %) was separately dissolved in ~2.75 mL of ethanol and then added to the TiO_2 sol solution. The precursor mixture was stirred for 12 h at room temperature to attain sufficient viscosity required for electrospinning. The solution was then loaded into a syringe connected to a stainless-steel needle of ~210 μm inner diameter. A direct-current (dc) electric field was applied between the needle and collector plate using a high voltage supply (Gauss High Voltage Research Inc. model RR50-1) that generates dc voltage up to 30 kV. The feed rate of the precursor solution was controlled

using a syringe pump (KDS 200). Samples were collected on aluminum foil flattened on a laboratory jack. Quartz and/or glass substrates (Asahi Glass Co.) placed over the aluminum foil were used for nanofiber collection for microscopic and optical measurements. The needle–collector plate distance was fixed at ~10 cm. Electrospinning was performed in a fume hood in air, whose humidity was maintained below 50%. The precursor solution was then electrospun at three conditions of applied voltage (kV) and flow rate (mL/h), i.e., (A) 10 kV and 1 mL/h, (B) 20 kV and 1 mL/h, and (C) 20 kV and 0.5 mL/h. During electrospinning, the applied electric field overcomes the surface tension of the polymeric solution, thereby ejecting a continuous jet, which upon subsequent solvent evaporation and bending produces nanofibers on the collector surface. The as-spun PVP–TiO_2 composite nanofibers were then annealed at ~120 °C for 12 h for drying and removal of the solvents. The annealed fibers were then sintered in the range 450–650 °C for 30 min (1) in a glass plate for electron microscopic measurements and (2) in a crucible for XRD measurements. The heating rate was fixed at 1 °C/min. The diameter and morphology of the PVP–TiO_2 precursor nanofibers as well as those annealed TiO_2 nanofibers were studied by using field-emission scanning electron microscopy (Quanta 200F) operating at 10 kV. Samples for scanning electron microscopy (SEM) were prepared by directly collecting the fibers on two glass plates for each spinning condition. One of the glass plates was maintained without heat treatment while the other was heated at ~500 °C for recording the SEM images of the as-spun and sintered fibers, respectively. The fiber diameters were measured from the SEM images using image analysis software (Image J1.29X). The sintered TiO_2 fiber surfaces were further examined by high-resolution transmission electron microscopy (HRTEM; JEOL 2010Fas) operating at 200 kV. Samples for HRTEM were prepared by ultrasonically dispersing the heated TiO_2 fibers in methanol and allowing a drop of this suspension to dry on a carbon-coated copper grid. The phase evolution and transition of the TiO_2 nanofibers were studied by an XRD technique using Ni-filtered Cu KR radiation (Shimadzu XRD-6000). The optical absorption spectra of the TiO_2 nanofibers were recorded using a UV–visible spectrophotometer (Shimadzu UV-1601) at a resolution of 1 nm. The photoluminescence (PL) spectra were recorded using a PL spectrophotometer (PTI photometer) by exciting the samples at 320 nm. Samples for optical measurements were obtained by directly collecting as-spun fibers on a quartz plate. The samples were first heated to 120 °C for 12 h and then to 500 °C for 30 min. The smooth TiO_2 nanofiber film deposited on the quartz substrate thus obtained was used for optical measurements.

Exp. Theo. NANOTECHNOLOGY 4 (2020) 1–10

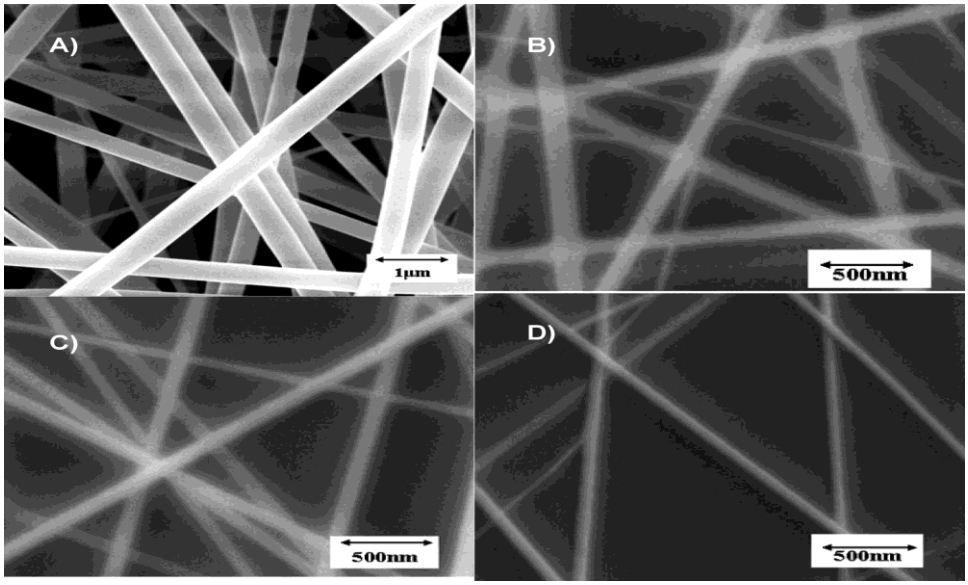

Figure 1 SEM micrograph of the (A) as-spun TiO_2−PVP composite nanofibers. Ceramic nanofibers with average fiber diameters of (B) 150 nm (10 kV and 1 mL/h), (C) 100 nm (20 kV and 1 mL/h), and (D) 60 nm (20 kV and 0.5 mL/h).

3. RESULTS AND DISCUSSION

Figure 1A shows a SEM image of TiO_2−PVP composite nanofibers electrospun at the (A) 10 kV and 1 mL/h condition from the ethanol/acetic acid/PVP/Ti(O^iPr)$_4$ solution. Each individual nanofiber maintained cross-sectional uniformity throughout the length, indicating a smooth injection of fine TiO_2 sol dispersed in the polymer matrix during electrospinning. The fiber diameter depended on the spinning conditions; the fiber diameters decreased with (i) an increase in the applied electric field and (ii) a decrease in the solution feed rate [20,23]. Average sizes of the as-spun fibers, which were measured from a sample of 100 fibers, were 450, 262, and 145 nm for the spinning conditions (A) 10 kV and 1 mL/h, (B) 20 kV and 1 mL/h, and (C) 20 kV and 0.5 mL/h, respectively. It is interesting to note that the electrospun fibers were 3 orders of magnitude less in diameter compared to that of the needle (~210 μm) through which the droplets were injected.

Parts B−D of Figure 1 show the morphology of the three sintered TiO_2 nanofibers developed by control of the initial electrospinning condition. These fibers have average diameters of 150, 100, and 60 nm for the spinning conditions (A) 10 kV and 1 mL/h, (B) 20 kV and 1 mL/h, and (C) 20 kV and 0.5 mL/h, respectively. The diameters of the sintered TiO_2 nanofibers were decreased to nearly one-third of those of the as-spun fibers. The PVP−TiO_2 composite fibers were sintered similarly to conventional metal oxide sintering: the binder burned off, and the pores thus created were filled by mass transport. The lowering of the fiber diameter on sintering is therefore partially due to the PVP evaporation and partially due to mass transport. The sintered TiO_2 nanofibers were dispersed in methanol and ultrasonically stirred to qualitatively examine the sintered density and mechanical strength of the fibers. The SEM images of the ultrasonically stirred fibers were the same as before, thereby indicating the mechanical strength and high sintered density of the electrospun TiO_2 nanofibers. The morphology of the TiO_2 nanofibers was further studied using HRTEM. Figure 2A shows a bright-field micrograph of a free-standing TiO_2 nanofiber of average diameter ~100 nm. The fiber surface was smooth and uniform, which indicates that TiO_2 was uniformly dispersed in the PVP mixture. The fibers

were polycrystalline and consisted of uniform grains of size ~12 nm. The grains were densely packed along the fiber length. The fiber cross section was a solid circle. Figure 2B shows a selected area electron diffraction (SAED) pattern recorded at 200 kV, which corresponded to an electron wavelength of 2.508 pm, and at a camera length of 1000 nm. The SAED pattern showed polycrystalline rings and was indexed for anatase TiO_2. No line corresponding to an impurity or secondary phase was detected. Figure 2C shows a typical HRTEM micrograph of the anatase TiO_2 nanofibers. HRTEM micrographs showed an alteration in the lattice periodicity along grain boundaries, which is possibly due to the lattice strains in the nanofibers. These lattice strains most likely originate from the interaction between the forces that bind the grains tightly together and the increased surface energy due to the nanocrystallinity of the particles.

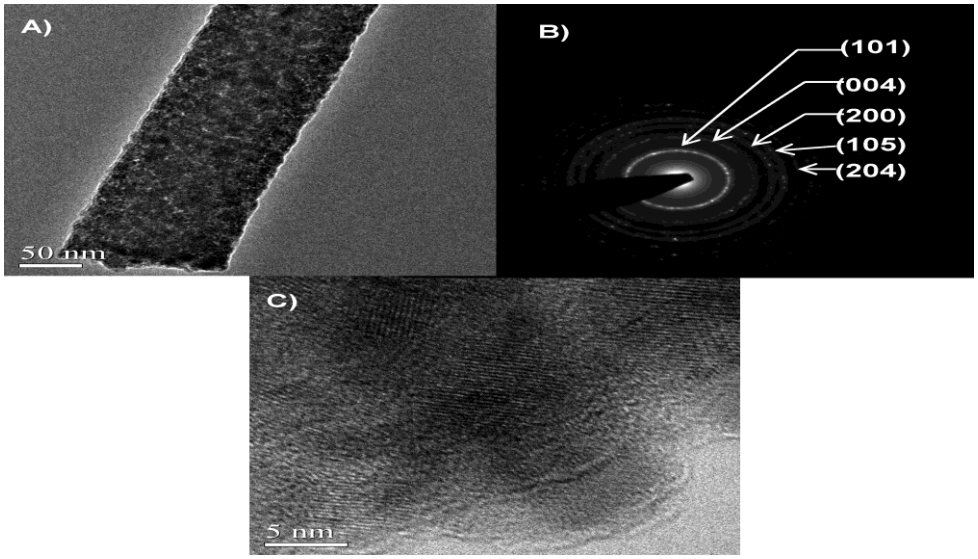

Figure 2 Bright-field micrograph of (A) free-standing anatase TiO_2 nanofibers of 100 nm diameter sintered at 500 °C. (B) Corresponding electron diffraction pattern. (C) HRTEM lattice micrograph of typical anatase crystallites showing strains.

To investigate whether the observed lattice strains have any effect on the optical properties of the nanofibers, we have recorded the absorption spectrum of the nanofibers. Figure 3A shows the UV absorption spectra of the nanofibers of diameters 60, 100, and 150 nm. The absorption peak was shifted from 320 to 335 nm when the fiber diameter increased from 60 to 150 nm. For nanometer-sized semiconductors, the shift of optical band gap originates from the quantum confinement effect and surface effects due to the higher surface energy of the nanofibers. Note that several authors have observed the blue shift in nanosized TiO_2 particles with

Exp. Theo. NANOTECHNOLOGY 4 (2020) 1–10

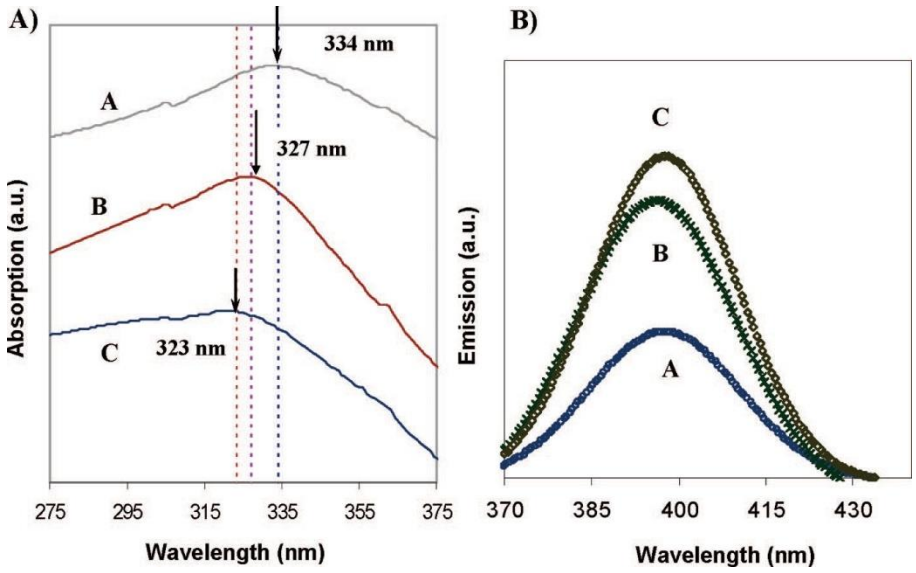

Figure 3 (A) Absorption spectra of TiO_2 nanofibers. (B) Corresponding PL spectra.

Anpo et al. [6] have reported the quantum confinement effect in the size regime of several tens of nanometers, whereas Serpone et al.[33] reported the confinement effect in TiO_2 particles of several nanometers. To the best of our knowledge, so far, no reports exist in the open literature on the effect of the fiber diameter on the electronic band gap of TiO_2 nanofibers. Remember that the size of the grains composing the fibers of different diameters were nearly the same in all of the fibers because of the lower sintering temperature and time; therefore, a size quantization effect is not likely the reason for the observed shift in the absorption spectra. Further, if a size quantization is the reason for the observed shift, a complementary shift would have been observed in their PL spectra. The PL spectra of these fibers exhibited a PL peak at ~400 nm and are not shifted with the fiber diameter (Figure 3B). A possible reason for the observed shift in the band-gap energy would be the surface stress associated with the surface energy of the nanofibers. Banfield et al. [10] have demonstrated that the stress and strain in nanoparticles strongly affect their functional behavior. These authors report that the surface stress induced structural disorders and the consequent changes in the lattice parameter in the nanoparticles occur even on chemically passivated surfaces. A stress-related band shift has been reported for heterojunction superlattices [34] and semiconductor ceramics [35]. Concerning bulk TiO_2, Camassel et al. [36] observed that the band gap increases because of the stress-induced breaking of the selection rule and resonance effects, when an external stress of several kilobars is applied [36]. In the case of nanofibers and nanoparticles, considerably high stress is likely to be generated by surface tension, which increases dramatically with decreasing nanofiber diameter/particle size. Thermodynamically, surface tension arises from the com- petition of surface atoms to attain lower energy states. A direct consequence of the surface tension is the compressive stress, the magnitude of which is inversely proportional to the radius of curvature. In the case of the TiO_2 nanofibers developed in the present work also, we observed an inverse relationship between the band gap and fiber diameter. The observed shift in the band gap is thought to originate from the surface stress due to the enhanced surface energy of these nanofibers. The surface stress strains the lattice and thereby stiffens the solid. The lattice strain and distortion give rise to band modification by breaking the selection rule[36] and/or by changing the Brillouin zone, in a way similar to that of the confinement-induced band modification [37]. Moreover, this stiffening of the surface-charge-induced stress affects the electron–hole mobility [34] and Ti—O binding energies, which, in turn, changes the band

structure. The surface stress in the electrospun TiO_2 nanofibers was calculated using the Laplace equation for excess pressure for circular cross section.

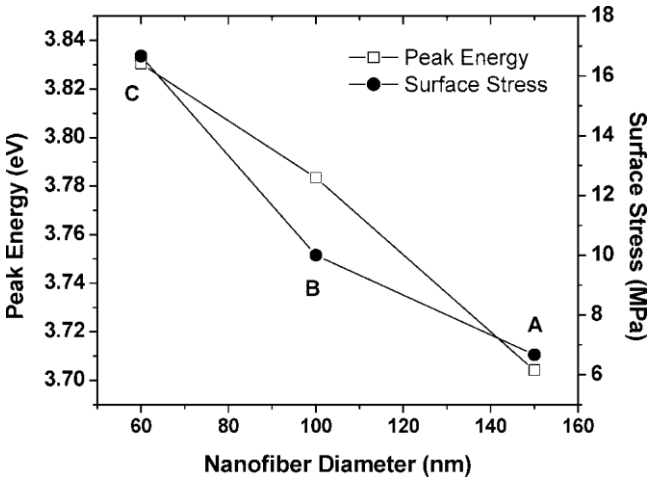

Figure 4 Variation of the excitonic peak energy and surface stress calculated based on the Laplace equation as a function of the fiber diameter.

Figure 4 that there is a clear relationship between the surface stress, fiber diameter, and band-gap energy of the nanofibers. The surface stress generates a strain in the fiber, the magnitude of which depends on the elastic constants of the fiber. Furthermore, we observed from the XRD patterns that the lattice strain decreases with an increase in the fiber diameter, consistent with the calculation of the surface stress. The results of fitting showed that fibers of lower diameter had higher strain values compared to fibers of larger fiber diameter. Indeed, the actual stress and strain and the associated phenomena such as lattice distortion and stacking faults [10] inside the nanofiber and the surface reconstruction at anatase TiO_2 surfaces [38] are rather complex and could not be accounted for by such a simplified model. Nevertheless, the simplified model and the self-consistent results presented here definitely prove the enhanced importance of surface energies at the nanometer scale.

4. CONCLUSIONS

In conclusion, the anatase TiO_2 nanofibers of variable diameters were fabricated by electrospinning of a polymeric solution and subsequent sintering. The sintered nanofibers were highly dense and polycrystalline and consist of uniform grains of average diameter ~12 nm. An anatase to rutile structural transformation occurred in the nanofibers at temperatures lower than ~570 °C. The rutile phase nucleated at the interface where an increased strain was observed as a result of the interaction between the surface energy and the forces that hold the grains together. These lattice strains were decreased with an increase in the fiber diameter. The surface stress in the fibers provoked a diameter-dependent shift in the absorption spectra. The excitonic peak showed a shift of ~15 nm when the diameter of the fiber increased from 60 to 150 nm. No complementary shift in emission spectra was observed; therefore, the shift in absorption spectra is unlikely due to the quantum size effect.

Exp. Theo. NANOTECHNOLOGY 4 (2020) 1–10

References

[1] F. M. Shamsudin, S. Radiman, Y. Abdullah, N. A. Hamid, Exp. Theo. NANOTECHNOLOGY 3 (2019) 27
[2] Fujishima, A.; Honda, K. *Nature* 238 (1972) 37
[3] O'Regan, B.; Gratzel, M. *Nature* 353 (1991) 737
[4] M. Devi, Manas R. Panigrahi, Exp. Theo. NANOTECHNOLOGY 2 (2017) 69
[5] Kormann, C.; Bahnemann, D. W.; Hoffmann, M. R. *J. Phys. Chem.* 92 (1988) 5196
[6] Anpo, M.; Shima, T.; Kodama, S.; Kubokawa, Y. *J. Phys. Chem.* 91 (1987) 4305
[7] Joselevich, E.; Willner, I. *J. Phys. Chem.* 98 (1994) 7628
[8] Lieber, C. M. *Solid State Commun.* 98 (1998) 607
[9] Peng, X.; M., L.; Yang, W.; Wickham, J.; Scher, E.; K., A.; Alivisatos, A. P. *Nature* 404 (2000) 59
[10] Gilbert, B.; H., F.; Zhang, H.; Waychunas, G. A.; Banfield, J. F. *Science* 305 (2004) 651
[11] Mikami, M.; Nakamura, S.; Kitao, O.; Arakawa, H.; Gonze, X. *Jpn. J. Appl. Phys.* 39 (2000) L847
[12] Kokubo, H.; Ding, B.; Naka, T.; Tsuchihira, H.; Shiratori, S. *Nanotechnology* 18 (2007) 1
[13] Bisma Bilal, Suhaib Ahmed, Vipan Kakkar, Exp. Theo. NANOTECHNOLOGY 3 (2019) 33
[14] Limmer, S. J.; Guozhong, C. *AdV. Mater.* 15 (2003) 427
[15] Miao, Z. Xu, D.; Ouyang, J.; Guo, G.; Zhao, X.; Tang, Y. *Nano Lett.* 2 (2002) 717
[16] G. Samla, K. B. Gan, S. M. Then, Exp. Theo. NANOTECHNOLOGY 2 (2017) 81
[17] Jun, Y. W.; Casula, M. F.; Sim, J.-H.; Kim, S. Y.; Cheon, J.; Alivisatos, A. P. *J. Am. Chem. Soc.* 125 (2003) 15981
[18] Wu, J.-M.; Han, C. S.; Wen, T. *Nanotechnology* 17 (2006) 105
[19] Tian, Z. R.; Voight, J. A.; Liu, J.; Mckenzie, B.; Xu, H. *J. Am. Chem. Soc.* 125 (2003) 12384
[20] Li, D.; Xia, Y. *Nano Lett.* 3 (2003) 555
[21] Huanga, Z.-M.; Zhangb, Y. Z.; Kotakic, M.; Ramakrishna, S. *Compos. Sci. Technol.* 63 (2003) 2223
[22] Sigmund, W.; Yuh, W. J.; Park, H.; Maneeratana, V.; Pyrgiotakis, G.; Daga, A.; Taylor, J.; Nino, J. C. *J. Am. Ceram. Soc.* 89 (2006) 395
[23] Li, D.; M., J. T.; Xia, Y.; Marquezz, M. *J. Am. Ceram. Soc.* 89 (2006) 1861
[24] ICDD Powder Diffraction Database, PCPDFWIN, PDF #211272.
[25] ICDD Powder Diffraction Database, PCPDFWIN, PDF #211276.
[26] A.M. Shehap, Kh.H.Mahmoud, M.F.H.Abdelkader, Tarek M.El-Basheer, Exp. Theo. NANOTECHNOLOGY 2 (2017) 103
[27] Zhang, H.; Banfield, J. F. *J. Mater. Res.* 15 (2000) 437
[28] Ranade, M. R.; Navrotsky, A.; Zhang, H. Z.; Banfield, J. F.; Elder, S. H.; Zaben, A.; Borse, P. H.; Kulkarni, S. K.; Doran, G. S.; Whitfield, H. J., *Proc. Natl. Acad. Sci.* 54 (2001) 54
[29] Ding, X. Z.; Liu, X. H.; He, Y. Z. *J. Mater. Sci. Lett.* 15 (1996) 1789
[30] Naser Al-Falahy, Omar Y. K. Alani, Exp. Theo. NANOTECHNOLOGY 3 (2019) 45
[31] Young, R. A., The Rietveld method. *International Union of Crystal-lography*; Oxford University Press: Oxford, U.K., 2002.
[32] Moser, J. Thesis No. 616, 1986.
[33] Serpone, N.; Lawless, D.; Khairutdinov, R. *J. Phys. Chem.* 99 (1995) 16646
[34] Smith, D. L.; Mailhiot, C. *ReV. Mod. Phys.* 62 (1990) 173
[35] Guerra, J.M.Stress-inducedbandgap–shiftedsemiconductor photoectrolytic/ photocatalytic / photovoltaic surface and method for making same.U.S. Patent, 2003.
[36] Camassel, J. Pascual, J. Mathieu, H. *Phys. ReV. B* 20 (1979) 5292

[37] P/ Peter, *Appl. Phys. Lett*. 37 (2011) 2547
[38] Lazzeri, M.; Selloni, A. *Phys. ReV. Lett.* 87 (2001) 266105

Exp. Theo. NANOTECHNOLOGY 4 (2020) 1–10